MDPI

Article

Ultrasonic-Assisted Granular Medium Forming of Aluminum Alloy 6063-T5: Simulations and Experiments

Han Hu [1,*], Feng Yu [1], Song Zhang [1], Jing Yin [1], Haiyan Zhang [1], Jiaru Zhang [1], Xiaonan Zhang [1], Miaoyan Cao [2,*] and Shahzad Murtaza [3]

1 Department of Mechanical Engineering, Ningbo University of Technology, Ningbo 315211, China
2 College of Mechanical Engineering, Yanshan University, Qinhuangdao 066004, China
3 Institute of Chemistry, Khwaja Fareed University of Engineering and Information Technology, Rahim Yar Khan 64200, Pakistan
* Correspondence: qyhmtrc@nbut.edu.cn (H.H.); jacmy@ysu.edu.cn (M.C.)

Abstract: To address the challenges posed by the complex shapes of hollow parts, this study examined the ultrasonic-assisted granular medium hydroforming (UGMF) process for tubular components. The dynamics of the deformation behavior and deformation control during 6063-T5 aluminum alloy tube free forming by UGMF were studied via simulations and experiments. Based on the ABAQUS software platform, a coupled method based on finite element (FE) simulation analysis and discrete element (DE) analysis for the UGMF free forming process was used. The results showed that ultrasonic vibration (UV) could reduce the forming force required for expansion and promote the flow of material at the end to the forming area as well as inhibit the decrease in the wall thickness. The accuracy of the FE-DE coupled simulation model and a parabolic geometric model was verified by testing. The results found that UV enhances material flow, decreases the forming force needed, and minimizes damage to the granular surface.

Keywords: tube forming; FE-DE; ultrasonic-assisted

1. Introduction

In the current era, the use of lightweight materials in the fields of aerospace and automotive materials has increased significantly to attain the goal of reducing emissions and energy, thereby improving efficiency. A light weight can be realized from two aspects: new materials and advanced manufacturing. The major drawback of using such lightweight material (aluminum alloys) is that it has poor formability at room temperature. With the increasing requirements for lightweight, high-strength, and high-performance products, thin-walled parts are being more commonly used in applications in the aerospace, medical, and automobile industries [1]. Aluminum alloys have been widely used in the tubular structure manufacturing of aerospace and automotive materials due to their low density, high specific strength, good electrical conductivity, good mechanical properties, and other advantages [2]. Due to the low forming properties of aluminum alloys at room temperature, the question of how to improve the forming properties of aluminum alloys has become a key area of research for many researchers [3]. Innovative forming methods such as solid granular medium forming (SGMF) have been proposed for industries throughout the world [3,4].

The difference between SGMF and the traditional soft die forming process lies in the different pressure transfer media and forming laws. The characteristics of strong heat resistance, easy sealing, small volume compression, no pollution to the environment, and green and non-uniform distribution of pressure transfer are used to improve the forming limit and forming performance [5]. However, when the targeted part is a complex component, the excessive forming force required in the forming process could crush the granules, leading to increased friction between granules, reducing inter-granule mobility,

and affecting the workpiece processing quality. This paper introduces ultrasonic vibration (UV) into SGMF technology, which might effectively reduce the forming force required and improve the workpiece forming quality. The technology is named ultrasonic-assisted granular medium hydroforming (UGMF) technology.

Ultrasonic-assisted forming processing has a wide range of applications [6]. Blaha et al. [7] applied UV to single-crystal zinc during tensile deformation and found that the flow stresses appeared to drop during ultrasonic action; after that, many scholars began to study ultrasonic-assisted metal forming, and the research on ultrasonic-assisted metal forming has come to the attention of research scholars. In an in-depth study of the UV tensile test and its forming mechanism, the ultrasonic-assisted forming process is applied to wire drawing, extrusion, piercing, punching, bending, deep drawing, and press forming processes, and it is based on the traditional drawing (tube drawing) process. The workpiece passes through the drawing (tube drawing) die at a certain speed, and UV with variable parameters is applied on the die. Many scholars have concluded that the use of the ultrasonic-assisted drawing process can effectively reduce the drawing force, improve the elongation coefficient of the tube, and improve the forming quality compared with the traditional drawing process [8]. Gao et al. [9] used a TA2 sheet to carry out a UV bulging test and found that appropriate UV parameters could effectively improve the forming limit of materials and inhibit spring-back. Zhai et al. [10] found that the surface effect of UV can effectively improve the friction condition between interfaces by using the double cup extrusion test under UV. Najafizadeh et al. [11] found that UV can improve the forming limit of sheet metal from macroscopic and microscopic perspectives, with a maximum increase of 28% in hardness and a 23% reduction in the average grain size of the specimens. Furthermore, Shahri et al. [12] indicated that applying UV improves metal flow and increases the corner filling ratio. Numerical and experimental analyses have already been performed in these studies on the application of UV on the deep drawing, upsetting, and bulging processes, etc., as shown in Figure 1, but few attempts have been made to investigate the effects of UV on the tube forming process so far.
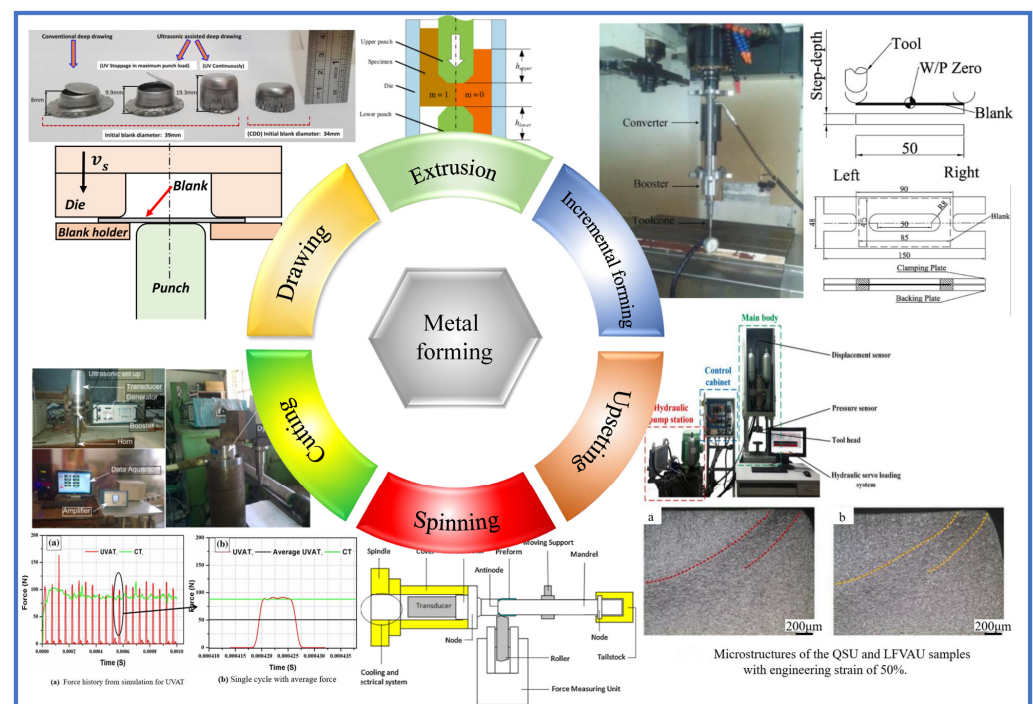

Figure 1. Development of future ultrasonic-assisted forming technologies [10,13–17].

The UGMF process involves the application of pressure and deformation of a tube by a discrete granular medium. A metal tube is a continuum body, and its forming

process and deformation characteristics under external loading conditions can be better analyzed using the traditional finite element (FE) method. Granules are a discrete and natural third-state material with characteristics of both solid and liquid states. In previous UGMF simulations, the Drucker–Prager (D-P) model has been used for the simulation of granules [18]. Although the results of the D-P model analysis are, in most cases, close to the theoretical calculation results and actual values, the discrete nature of the granules cannot be reflected due to the treatment of the granular medium as a continuum, and the large deformation generated by the medium during the forming process makes the mesh of the D-P model extremely susceptible to distortion and operation termination, which affects the calculation accuracy. The discrete element (DE) method is the most effective analysis tool for granules [19–22] as it has advantages over other methods in reflecting the discrete nature of granules and revealing the structure of the internal force chain, the contact deformation between granules, and the force transmission characteristics of granules. A finite element–discrete element (FE-DE) coupled numerical model is developed in this study which accounts for both the deformation behavior of the tubular blank (continuum, FE) and the mechanical characteristics of the granular filler (discrete medium, DE) [23]. The FE-DE method has significant advantages in forming processes [24].

This FE-DE method is used to study the free forming process of tubes under UV to investigate the forming mechanism based on the UGMF process more realistically and accurately. The granular model is used in ABAQUS 2022 software to analyze the UGMF via the FE-DE model. Then, the forming force, wall thickness, and strain history during the tube forming under UV are analyzed through geometric analysis models and FE-DE coupled simulations. Based on the advantages of UGMF technology, the paper focuses on the UGMF process and how the use of UV affects formability. The accuracy of the FE-DE coupled model is proven from an experimental viewpoint, and the results show that the application of UV can reduce the forming forces on tubes and promote the material flow.

2. The Mechanism of Transverse UV Forming

The schematic diagram of the UGMF process of a thin-walled tube under free forming is illustrated (Figure 2). In the conventional forming process, the die is stationary, and the tube wall is compressed and deformed by the granules. The upper die undergoes transverse UV in the UGMF process. The transverse UV in the densification process can also generate better arranged and less fractured structures with a uniform density distribution about the granular medium [25,26]. Notably, the UGMF process first takes advantage of the strong pressure-bearing capacity, simple filling ability, and recyclability of the granular medium [27].
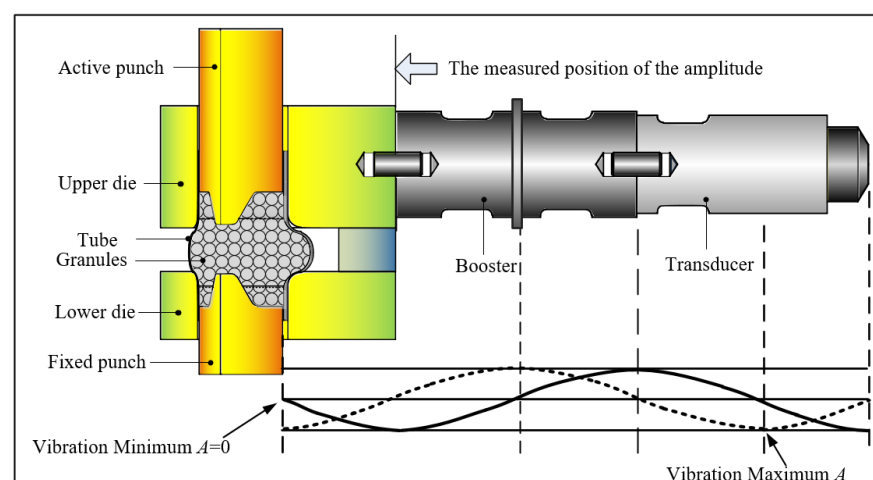

Figure 2. The principle of UGMF bulging.

2.1. Vibration Modal Analysis

As the shape of the upper die is annular, the amplitude of the inner wall of the ring cannot be detected by a traditional laser vibrometer. It is known that the structure of the UV system mainly includes four parts: an ultrasonic generator, a transducer, a booster, and a ring (in this study, UV was applied on the upper die) [28]. In this paper, the frequency of the ultrasonic transducer was 20 kHz. The optimal size of the ring was obtained using the optimization design function of the finite element analysis software ABAQUS, and the modal analysis of the ring vibration system was carried out to obtain the amplitude displacement amplitudes in the middle of its displacement ring.

2.2. Die Design and Modal Analysis on UV

Since the ultrasonic generator cannot oscillate, the ultrasonic energy cannot be effectively applied to the desired formed tube; thus, it was necessary to design a variable-amplitude rod (straight type) and a ring-shaped upper die with an amplification factor of 1, and its dimensions are referenced in the literature [29]. The upper die was circular in shape due to the use of a non-traditional variable-amplitude rod. The inner diameter of the ring was fixed at 50 mm, with the outer diameter and height of the ring being design variables and the frequency f being the state variable. The specific dimensions of the circular upper die were obtained through modal analysis, and its shape was optimized and further designed to obtain the final test die. Its specific structure is shown in Figure 3. To better determine the vibration form of the circular upper die during the forming process and to analyze it specifically, the material of the circular upper die was selected as 45#, with the following material parameters: density ρ = 7840 kg/mm^3, E = 2.16 × 10^{11} N/mm^3, and v = 0.28. For the frequency simulation analysis step, the number of features was set to 40.
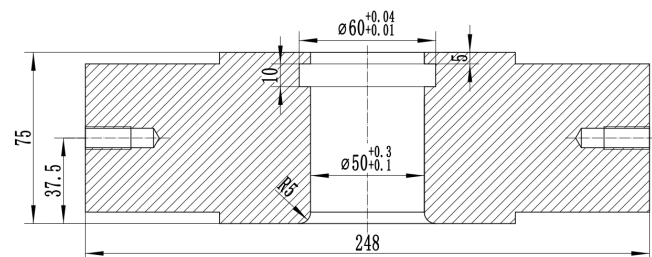

Figure 3. Upper die of UGMF test device of 6063-T5 aluminum alloy.

Figure 4 shows the modal vibration patterns which were obtained from the modal analysis of the ring upper die with ABAQUS 2022 software. By observing the vibration mode of the vibration system at around 20 kHz frequency, it was found that among the three adjacent vibration patterns, except for the 32nd-order vibration pattern with a frequency f = 20.242 kHz, the other two vibration patterns could not concentrate the vibration energy to the inner cavity surface of the die, and the maximum flow direction of the vibration oscillator is shown in Figure 4b. The figure shows the reciprocating direction of the inner cavity of the die, which was the vibration pattern required for the test. Then, Figure 4d shows the one-dimensional reciprocating vibration mode for a period T of the upper die. The die provided active friction reciprocally as well as hindering friction.
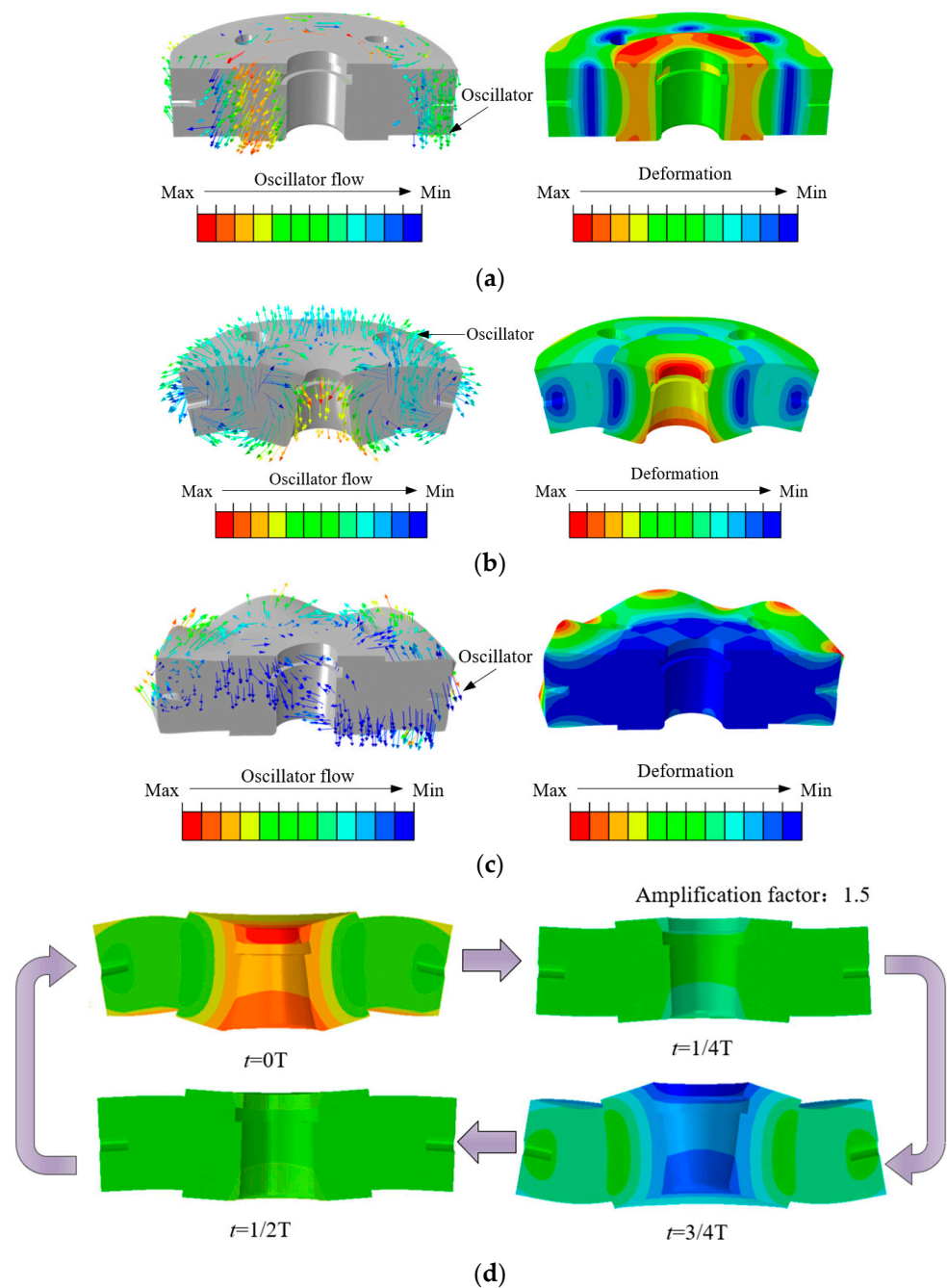
Figure 4. Upper die mode shape diagrams. (**a**) Mode number 31, *f* = 19.766 kHz. (**b**) Mode number 32, *f* = 20.242 kHz. (**c**) Mode number 33, *f* = 20.993 kHz. (**d**) Schematic diagram of one-dimensional reciprocating vibration mode of upper die (*f* = 20.242 kHz).

2.3. Measurement of UV Amplitudes

Figure 2 shows the diagram of the UGMF test with UV applied, where the ultrasonic generator, transducer, and booster transmit ultrasonic energy to the upper die, which is transmitted to the surface of the tube. Based on the results in Section 2.2, the displacement amplification between the contact surface and the inner wall of the circle was calculated to be 1.15. Thus, by measuring the amplitude of the variable-amplitude rod, the amplitude of the inner wall of the upper die in contact with the tube could be indirectly obtained. An SOPTOP-LV-S01 series laser vibration meter measured the ending amplitude of the booster, as shown in Figure 5, and its different gear amplitudes are shown in Table 1.
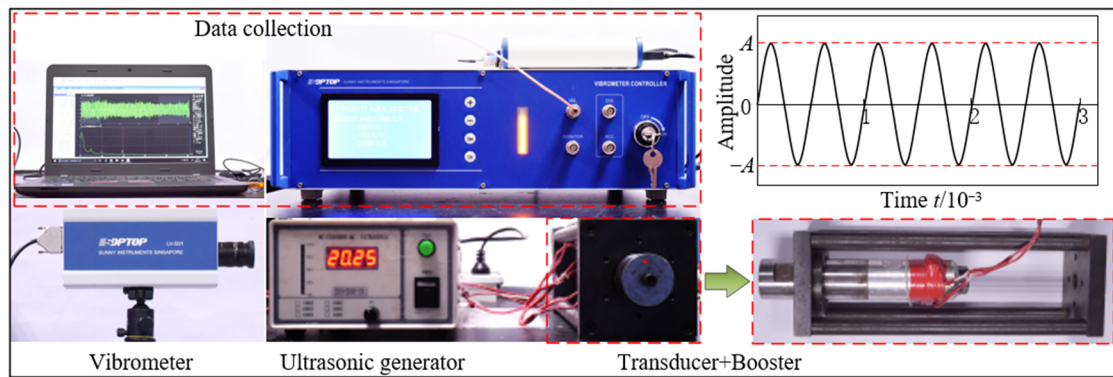
Figure 5. SOPTOP-LV-S01 series laser vibrometer.

Table 1. Amplitude of horn under different UV.

Level	0	I	II	III
Amplitude of booster (μm)	0	2.2	3.6	4.9
Amplitude of upper die (μm)	0	2.5	4.1	5.6

2.4. Geometrical Model

The tube was free to deform under the internal pressure of the granules, friction reduction was achieved via UV, and the target workpiece was obtained. In this study, the unprocessed tube was taken as the initial state. The pressure of the active punch was transferred to the granules, and the free bulging area expanded outward and deformed until the film was attached. The combined effect of the tensile force in the free bulging region, the granular friction, and the friction reduction effect at the contact between the tube and the upper die caused by the UV resulted in the flow of material from the upper end of the tube towards the free bulging region. As the lower end of the tube was fixed during free forming, greater internal pressure was required to form the shape of the outer contour of the wall with free distribution. The sketch of the deformation is shown in Figure 6.
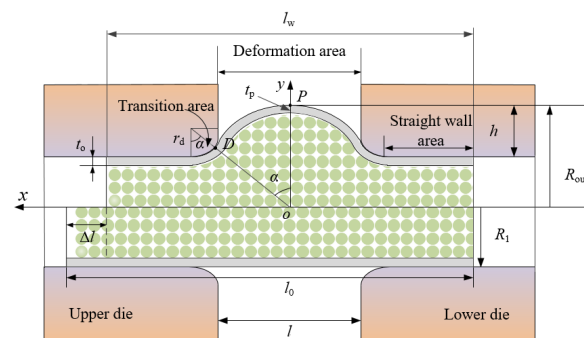

Figure 6. Geometrical model of free bulging.

Let the shape function of the free bulging region (the tube not in contact with the die) in the *xoy* coordinate system be as follows:

$$y = bx^2 + R_{\text{out}} \tag{1}$$

where D (x_D, y_D) is the contact point between the free bulging area of the tube and the concave die, which can be obtained according to the continuous curve at point D:

$$x_D = \frac{l}{2} + r_{\text{d}}(1 - \sin\alpha) \tag{2}$$

$$y_D = R_1 + r_{\text{d}}(1 - \cos\alpha) \tag{3}$$

$$b = \frac{y_D - R_{\text{out}}}{x_D} = \frac{R_1 + r_{\text{d}}(1 - \cos\alpha) - R_{\text{out}}}{\frac{l}{2} + r_{\text{d}}(1 - \sin\alpha)} \tag{4}$$

where R_1—initial outer radius (mm); r_{d}—radius of die fillet (mm); l—length of free bulging area (mm); R_{out}—forming height of point P (mm); α—angle of die attachment in the transition area (°); b—coefficient of the parabolic quadratic term.

According to the constant volume before and after bulging, the following formula can be obtained:

$$2\pi\left[\int_0^{x_D} y^2 dx - \int_0^{x_D}(y-t)^2 dx + \int_0^{\alpha}(R_1 + r_{\text{d}} - r_{\text{d}}\cos\theta)^2 r_{\text{d}} d\theta - \int_0^{\alpha}(R_1 + r_{\text{d}} - r_{\text{d}}\cos\theta - t)^2 r_{\text{d}} d\theta\right] + \pi(R_1^2 - R_0^2)(l_0 - l - \Delta l) = \pi(R_1^2 - R_0^2)l_0 \tag{5}$$

where R_0— initial inner radius (mm); l_0— initial length (mm); Δl—length of end shrinkage (mm); t—wall thickness after expansion (mm). Due to the small change in t in the bulging process, its value can be considered as the original wall thickness t_0. Then, according to Equation (5), the contraction length at the end can be written as follows:

$$\Delta l = \frac{\frac{4}{3}t_0 - x_D^3 + (4t_0 R_{\text{out}} - t_0^2)x_D + 2\alpha r_{\text{m}}(2R_1 + 2r_{\text{d}} - t_0) - 2r_{\text{d}}^2\sin(\alpha)}{R_1^2 - R_0^2} - l \tag{6}$$

3. Simulation Analysis

3.1. Unidirectional Tensile Test under Transverse UV

The finite element software ABAQUS 2022 was used to simulate the free forming process with UV. The FE-DE model in this paper was established based on the literature. The mechanical properties of the 6063-T5 aluminum alloy under UV are different from the traditional mechanical properties. A transverse UV tensile test system was designed based on WDW-100 kN universal testing apparatus. The UV equipment had a fixed frame and provided ultrasound with a frequency of 19.81 kHz by an ultrasonic generator, in which the maximum power is 3000 W. The UV was delivered to the specimen through a piezoelectric ceramic transducer, booster, and punch (Figure 7a), which were fixed to a slide, and elastic devices were installed on both sides of the experimental setup to ensure the effective transmission of UV. In the tensile test, the output power of the UV generator was adjusted to realize the excitation of different UV energy fields on the specimen. The experimental results are shown in Figure 8.
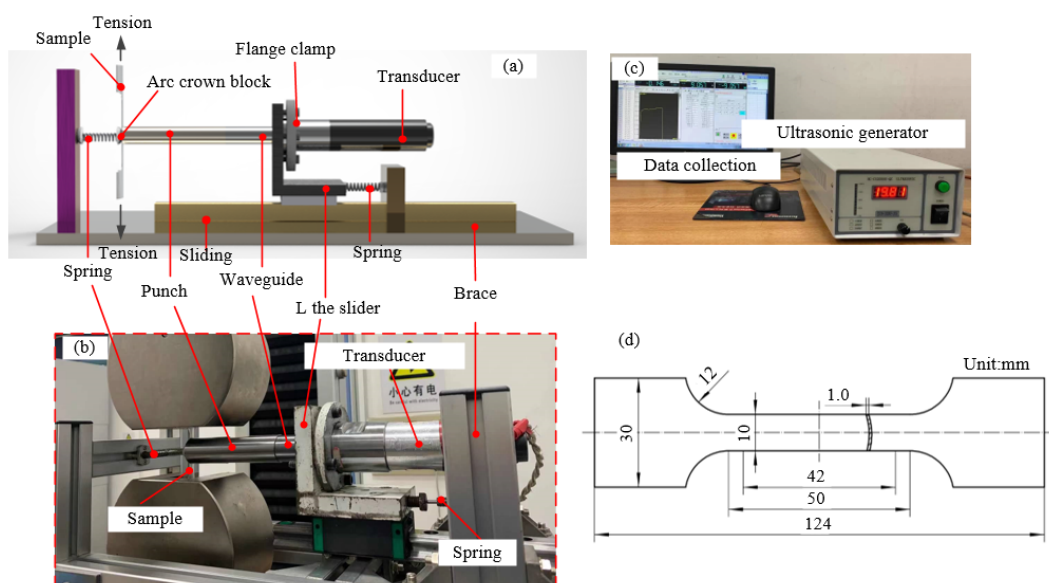

Figure 7. Equipment of transverse ultrasonic-assisted tensile tests. (**a**) Experimental setup schematic. (**b**) Experimental setup. (**c**) Data collection setup. (**d**) Sample size.
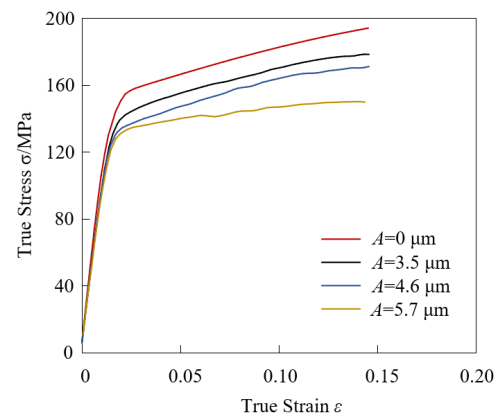
Figure 8. True stress–strain curves of 6063-T5 tubular specimens under different UV amplitudes.

Based on the Holloman equation $\bar{\sigma} = K\bar{\varepsilon}^n$ [30], the material properties under UV were fitted, where K is the strength coefficient and n is the hardening index. The values for different amplitudes are shown in Table 2.

Table 2. Value table of K and n at different amplitudes.

A/μm	K	n
0	223.34	0.0706
3.5	201.72	0.0645
4.6	186.18	0.0567
5.7	160.32	0.0362

3.2. FE-DE Model

In this study, ABAQUS 2022 was used to implement an FE-DE coupled method to determine the real-time influence and interactions between the granular motion and metal deformation. The simulations considered not only the influence of the metal tube on the granular motion but also the influence of granules on metal deformation. The DEM was used in ABAQUS to analyze the UGMF process of the 6063-T5 tube. The simulation model is shown in Figure 9.
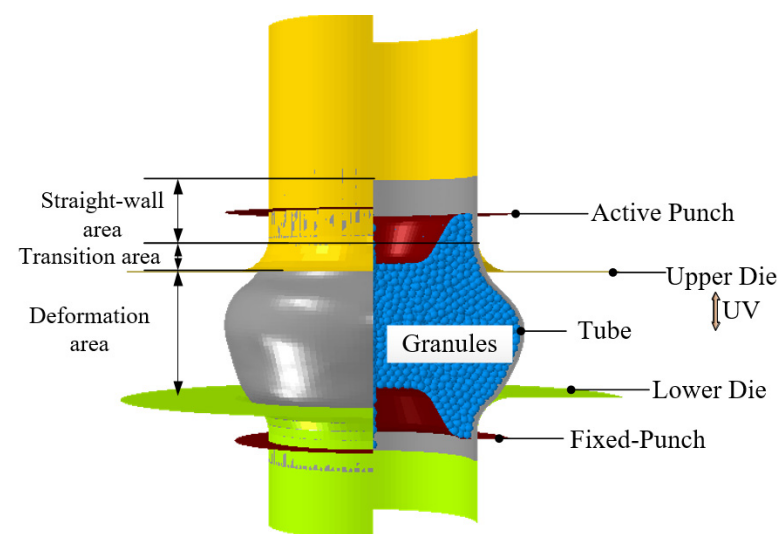

Figure 9. FE-DE coupling model.

3.2.1. Modeling

The tube was a deforming body composed of shell elements. The dies and punches were modeled as rigid bodies to save time. A four-node quadrilateral finite film strain-linearly reduced integral shell element (S4R) was used to simplify the whole shell element in the numerical simulation model. The granular model was directly generated in the ABAQUS 2022 visual interface by a self-programmed embedded subroutine, and the continuum body unit C3D8R was modified to PD3D. The granular radius was 1.0 mm. Each PD3D unit contained a node with six degrees of freedom. The granular medium model consisted of any spherical particles, whose information was specified in an INP file through an input template [31]. The mixed modeling of granules was established by assigning different radii and densities to different node geometries.

3.2.2. Materials

The die and granule materials are shown in Table 3. In the simulation, it was necessary to introduce the true stress–strain curve of the material under UV. Thus, tension tests were performed. Table 2 shows the true stress–strain relation obtained for the material under UV, which reflected the volume effect in the simulation.

Table 3. Parameters of model simulations.

	Young's Modulus/MPa	Density/kg·m^{-3}	Poisson's Ratio
6063-T5	6.90×10^4	2720	0.33
Die	2.08×10^5	7850	0.27
Granules	7.20×10^4	25	0.20

3.2.3. Boundary Conditions and Loading

The steps of the simulation were as follows.

Step 1: The granular medium in this model is subjected to gravity loading.

Step 2: The punch is moved to deform the tube. The displacement of the punch is defined as *S*, and *t* is replaced by the periodic amplitude curve time in the bulging process of the tube, which is set on the upper die. The analytical formula of the amplitude curve is shown in Equation (7):

$$y = A \sin(2\pi f t) \tag{7}$$

where *y* is the displacement of the UV, and *A*, *f*, and *t* are the amplitude, frequency, and time of UV, respectively. The UV changed the contact state between the upper die and the tube, which reflected the volume effect in simulation.

3.2.4. Interactions

The volume effect of the tube under UV could not be accurately described in the module of ABAQUS/Explicit module. The FE-DE coupled model had three kinds of contacts, including contact between granules and contact between the die and the granules. The friction coefficients for the contact between the granules and the contact between the granules and the die/tube were consistent with the friction test results [32]. Based on the granules in ABAQUS, general contact was adopted for the large number of contacts between the granules. The original friction coefficients are shown in Table 4.

Table 4. Original friction coefficients of the model.

Contact Pairs	Tube–Die	Granules–Granules	Tube–Granules
Coefficient of friction	0.10	0.3	0.2

4. Analysis of Result of Finite Element Simulation

The frequency and amplitude affected the results of the simulation. To obtain the influence of UV on the forming process, the UGMF free bulging of tubes was analyzed based on the FE-DE coupled model by changing the above process parameters.

For the UV, its influence parameters mainly included frequency and amplitude. Therefore, to further study the influence of UV on the UGMF process of the tube, firstly, the solid granular medium forming of the tube was studied by changing the frequency value. The frequencies selected were f = 20 Hz, 200 Hz, 2 kHz, and 20 kHz. The amplitude A = 4 μm was used to study the influence of frequency on the change in tube wall thickness. Figure 10b shows the variation curve of the tube wall thickness at different frequencies. The wall thickness values corresponding to vibration frequencies of f = 20 Hz, 200 Hz, 2 kHz, and 20 kHz were t = 0.894 mm, 0.895 mm, 0.895 mm, and 0.899 mm, respectively, indicating that there was little difference in minimum wall thickness. Therefore, the frequency of UV has little influence on the minimum wall thickness of the tube.
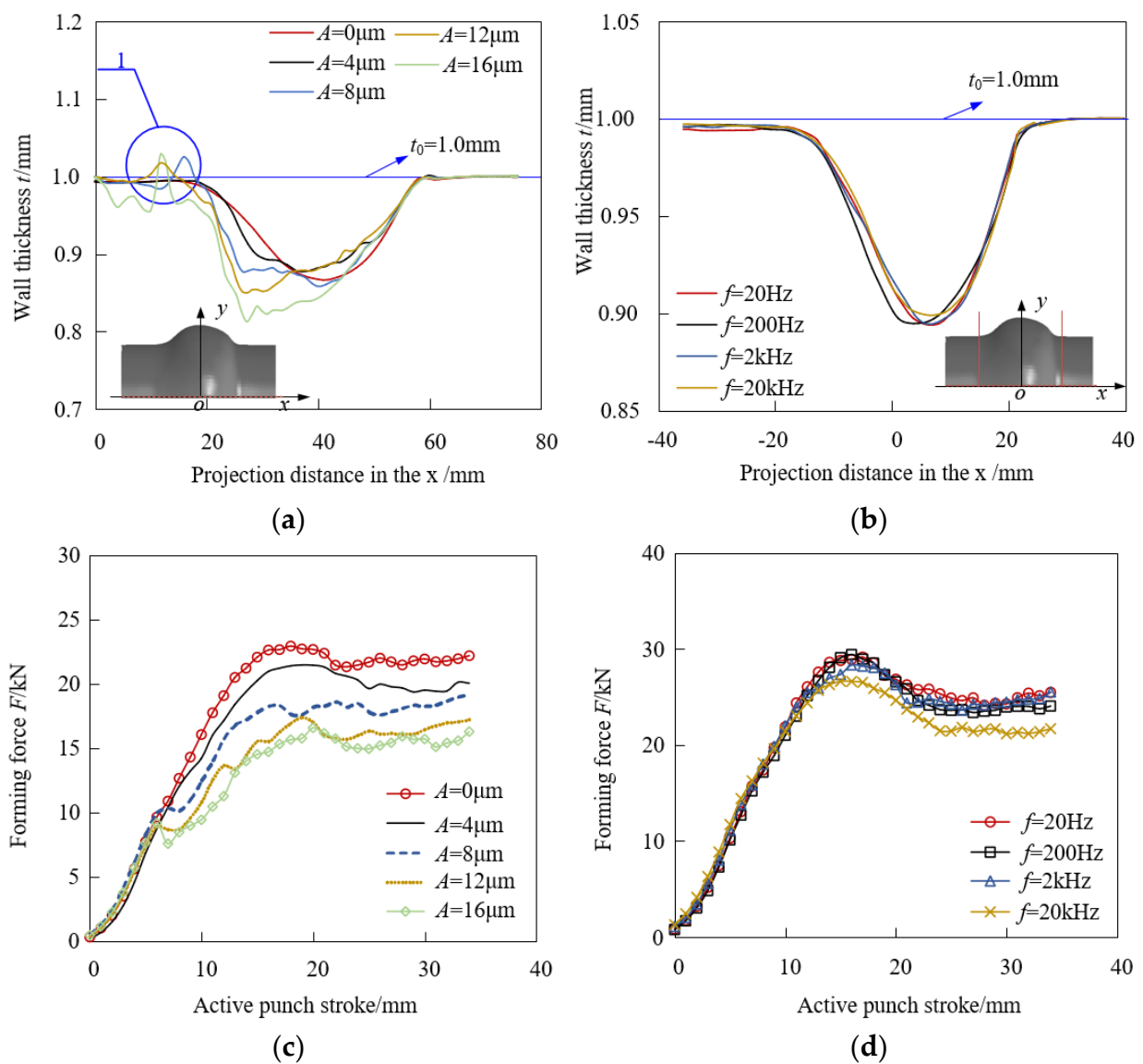

Figure 10. The curve of wall thickness and force forming under different transverse UV conditions. (**a**) Wall thickness under different frequencies. (**b**) Wall thickness under different amplitudes. (**c**) Force forming under different frequencies. (**d**) Force forming under different amplitudes.

In this study, the influence of UV on the forming process was examined. Therefore, f = 20 kHz was selected as the simulation condition to study the influence of vibration amplitude on the wall thickness of the formed parts, as shown in Figure 10a. It was found that when the amplitude A = 0, 4, 8, 12, and 16 μm, the minimum wall thicknesses of the corresponding tubes were 0.866, 0.877, 0.859, 0.852, and 0.841 mm, respectively. When the amplitude A = 8~16 μm, the wall thickness of the tube began to shrink significantly, and the wall thickness of the tube near the vibration source fluctuated. This is because during the simulation process, the contact between the upper die and the tube was in the form of a reciprocating motion that momentarily promoted and then impeded the flow of the tube material. As the expansion proceeded, the diameter of the straight wall section of the tube increased slightly due to the granules, while the equilibrium position of the die was fixed. This impeded the contact between the straight wall section of the tube and the die, affecting the flow of material from the straight wall section of the tube to the deformation area and causing the wall thickness of the deformation zone and straight wall section to fluctuate, as in region 1. The wall thinned significantly as the amplitude increased. When the amplitude A = 4 μm, it can be seen that the tube wall thickness changed uniformly, and the minimum wall thickness was greater than that at A = 0 μm. This is because when the amplitude was small, the obstructing effect of the die on the straight wall section of the tube was smaller. At the same time, its promoting effect was significant, which helped the material of the straight wall section of the tube to flow to the deformation area and made the wall thickness of the tube change more uniformly.

Figure 10c,d show the forming force supplied by the active punch to the granules under different frequencies and amplitudes, which can be called the forming force required for the tube expansion. The forming force size affected the required equipment requirements. The displacement Q of the active punch was set to 37 mm and the amplitude A = 4 μm was selected. Under the same amplitude, with the increase in frequency, the required forming force was reduced. When the frequency f = 20 kHz, belonging to the ultrasonic frequency range, the reduction in the forming force was more significant, and the maximum difference in the forming force was 3.81 kN. For the subsequent analysis of the ultrasonic-assisted granular medium forming process, the tube was set to a frequency of f = 20 kHz.

5. Experimental Validation of the Process and Analysis

Simulations of the conventional forming and UGMF processes were performed primarily. To validate the simulation results, a comparison was made between the numerical simulation results and the test results.

5.1. Experimental Equipment

To verify the feasibility of the tube UGMF free forming process, a forming die and a transverse UV forming device were designed and manufactured according to the principle of the forming process. The test process of the UGMF is shown in Figure 11. The main active tool components were punches, dies, a UV system, granules, and a tube, which had a 50 mm initial diameter, 80 mm length, and wall thickness t_0 = 1 mm. During the forming process, the active punch was controlled by a 100 kN universal tensile testing machine. The digital image correlation (DIC) online measurement system used for the test was the VIC-3D non-contact full strain measurement system. The system was developed by China Thousand Eyes Wolf Company, and it uses a DIC algorithm (Figure 11a). Before conducting the test, black and white scattered spots were sprayed on the surface of the tube, and during the forming process, an industrial camera was used to collect the image information at a rate of 5 shots/s. The primary purpose of designing the active punch was to compress the granular system, and the forming die contact with the blank provided support for the upper die. Under the constraints of the punch, granules, and dies, the tubes freely deformed. The different levels of deformation corresponded to the UV amplitude, as shown in Table 1.
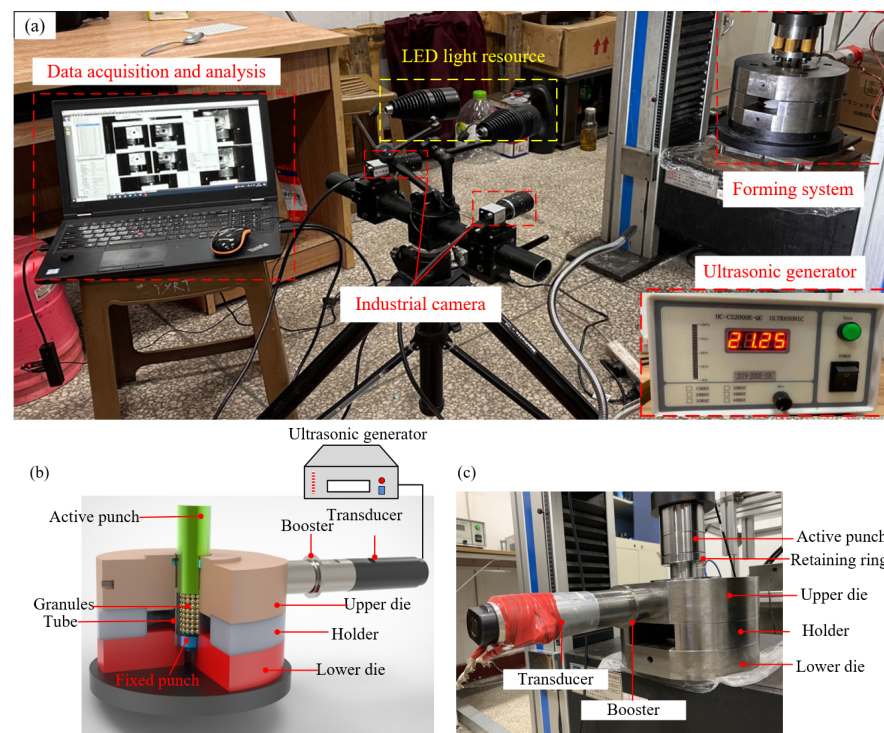
Figure 11. Experimental setup of UGMF. (**a**) Test process of UGMF. (**b**) Schematic diagram of UGMF. (**c**) UGMF test equipment.

5.2. Experimental Results and Discussion

5.2.1. The Effect of UV on the Forming Force

Taking the free expansion of the tube as an example, the forming force caused by the active punch extrusion granules to deform the tube in the free expansion process under the UGFM process was analyzed. When the forming force reached 24 kN, the loading was stopped, as shown in Figure 12. During the forming process, UV was applied either over the whole process (Figure 12a) or intermittently every 15 s (Figure 12b).
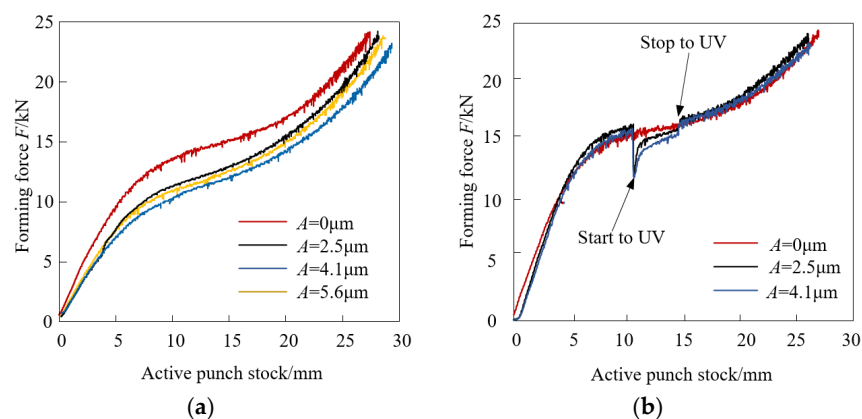

Figure 12. Force curve of simulation and test under different amplitude. (**a**) Whole process with UV. (**b**) Process with intermittent UV.

As can be seen from Figure 12a, the forming force curve fluctuated during in the forming process. This was because with the continuous increase in the forming force of the active punch, the extrusion force on the granules increased, exceeding the compressive strength of the granules and resulting in granule breakage, which was accompanied by a sound. When UV was applied, it could improve the fluidity of the granules, so the granules

were constantly rearranging to form a new structure in the process of UV application, thus increasing the compression capacity and delaying granule breakage. As a result, the curve fluctuation amplitude of the forming force was reduced. As shown in Figure 12b, at the moment when UV was applied, the forming force decreased instantaneously but then gradually increased. However, it remained smaller than with no UV. When the UV was stopped, the change in the forming force began to return to the state under no UV. Therefore, it can be seen that the application of UV could reduce the forming force required by the forming part.

In the process of tube production, a scanning electron microscope (SEM) was used to observe the morphologies of the granules after the sound of granule fracture. Figure 13 shows the morphologies of the granules under different UV conditions. In the forming process, since there were pores between the granules when the granules were the forming medium, the active punch first compressed the granules, thus reducing the porosity. With the continuous movement of the active punch, the required forming force gradually increased, and the granules could not bear it, resulting in surface damage, as shown in Figure 13c. The forming force curve fluctuated at the moment of granule surface fracture (Figure 13). When UV was applied in the forming process, the granules constantly rearranged to fill the pores between the original granules. Under UV, the pores between the granules reached the minimum size. At the same time, due to the application of UV, the granules bonded, and the compression resistance of the granules was enhanced, as shown in Figure 13d,e. Therefore, UV applied in the forming process could delay the fluctuations in the forming force curve and improve the cracking resistance of the granules. The results showed that UV could not only reduce the forming force but also restrain the fracture of granules to a certain extent.
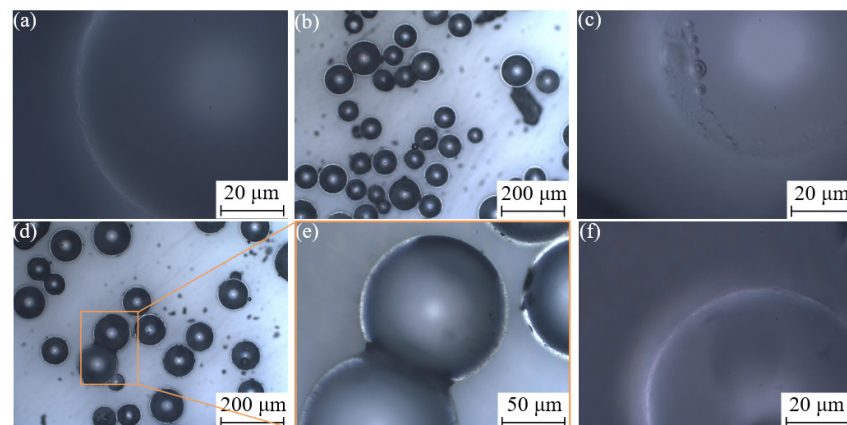

Figure 13. State of granules under different transverse UV conditions. (**a**) Untreated single granule. (**b**) State of granules after compression under A = 0 μm ($P(x)$ = 24 kN). (**c**) Single granule's surface morphology under A = 0 μm ($P(x)$ = 24 kN). (**d**) State of granules after compression under A = 4.1 μm ($P(x)$ = 24 kN). (**e**) Granules bonding under A = 4.1 μm ($P(x)$ = 24 kN). (**f**) Single granule surface morphology under A = 4.1 μm ($P(x)$ = 24 kN).

5.2.2. The Effect of UV on the Forming Force

During the expansion of the 6063-T5 tube during UGMF, three forms of vibration were compared: (1) without UV; (2) with UV; (3) with intermittent UV (an intermittent vibration for 15 s duration during the free forming process). The three modes were used to record the tube forming to fracture and the strain state at the fracture. The DIC system detected the strain of the tube during the bulging process (Figure 11a). After the forming and fracture, the system software was used to calculate the strain distribution and historical changes. A test was conducted to determine the strain values at the fracture zone of the 6063-T5 aluminum alloy under UV. The 6063-T5 tube fracture zone under UV was experimentally

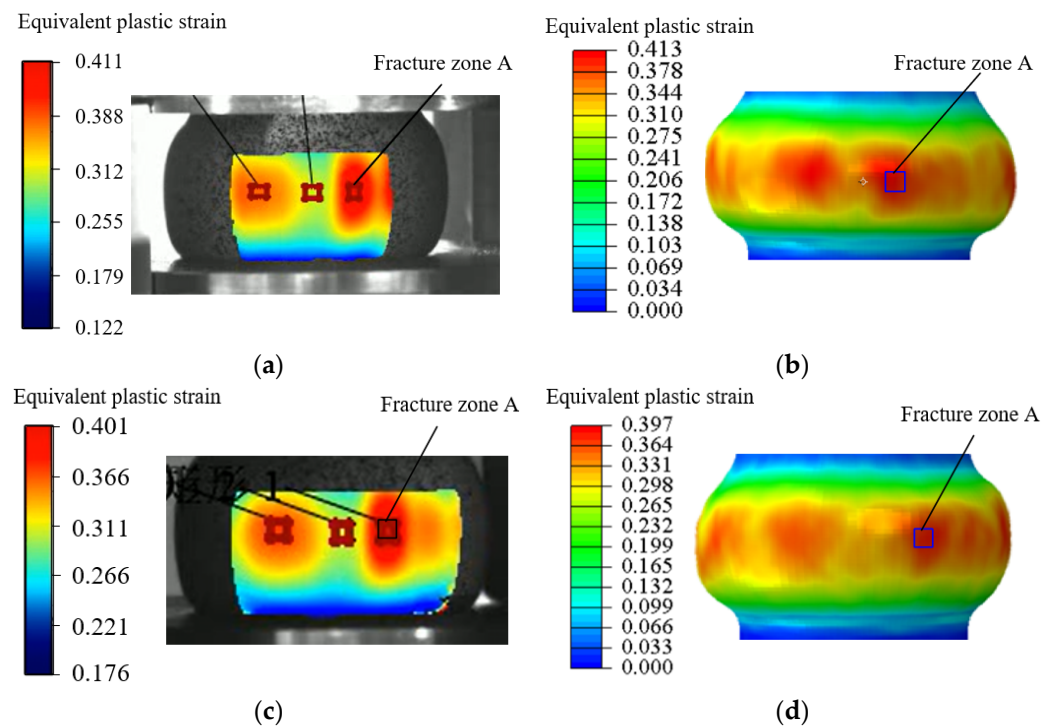collected and compared with the coupled FE-DE model established in Section 4, as shown in Figure 14.

Figure 14. The strain distribution obtained by the DIC system. (**a**) $A = 0$ μm, DIC strain distribution. (**b**) $A = 0$ μm, FE-DE coupled strain distribution. (**c**) $A = 4.1$ μm, DIC strain distribution. (**d**) $A = 4.1$ μm, FE-DE coupled strain distribution.

Figure 14 shows that the strain distribution of the tube obtained by the DIC system was consistent with the strain distribution simulated by the coupled FE-DE model, which could further prove the validity of the coupled model.

5.2.3. Effect of Vibration on Strain

The results for the case where UV was applied throughout the forming process are shown in Figure 12a. UV was applied to the forming process according to Figure 14b, at the forming expansion time of 42 s. The specimen vibration lasted for 15 s, and then the UV application ended. The area at the rupture, labeled as Zone A in Figure 14, was selected as the strain history point for observation, and the results are shown in Figure 15.

As shown in Figure 15b,d, the DIC strain detection provided the same trend of strain history as the coupled FE-DE model, which further proves the validity of the coupled model. By comparison with Figure 15a, it can be seen that the application of vibration reduced the forming force on the whole. As shown in Figure 15a, the strain rate of the corresponding strain curve decreased, and the hardening of the tube during deformation was weakened, which could improve the forming limit of the tube to a certain extent. Comparison with Figure 15b shows that the application of vibration caused the forming force to appear to decrease sharply, and with the increase in time, the forming force when the vibration was stopped returned to the state when UV was not applied. For the strain field of the tube, when UV was applied, the strain in the same area decreased, changing the strain rate during the expansion process, and when the vibration was stopped, the strain state gradually returned to the state when UV was not applied. In summary, the application of UV could reduce the strain rate during the forming process to some extent, thus affecting the expansion process.
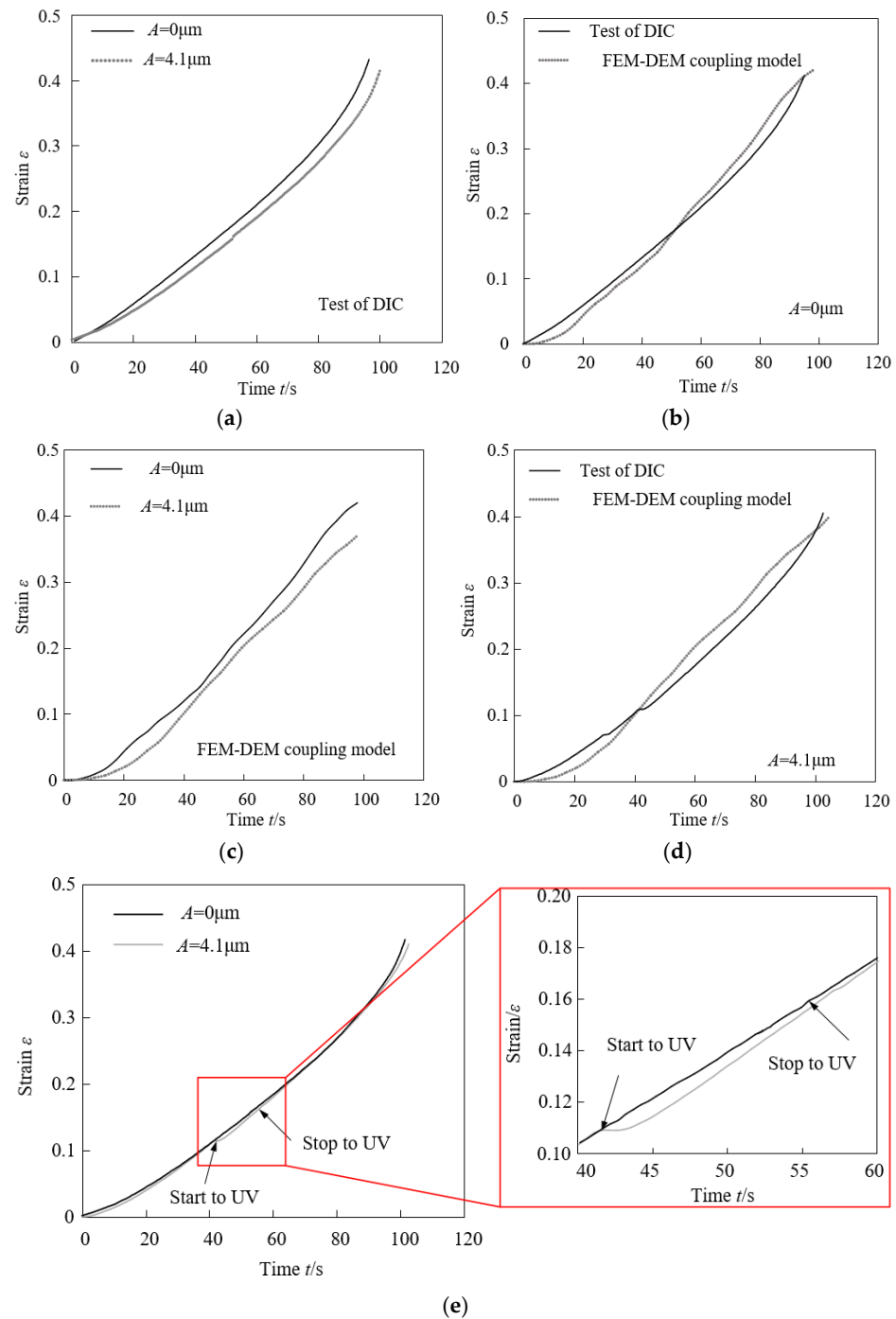
Figure 15. Strain history of tube forming under $A = 0$ μm and $A = 4.1$ μm. (**a**) Contrast curve of strain with different A values. (**b**) Experimental and simulated strain curves. (**c**) Contrast curve of strain with different A values. (**d**) Experimental and simulated strain curves. (**e**) DIC strain distribution (test).

5.2.4. The Effect of UV on the Wall Thickness

Figure 16 shows the distribution of the wall thickness under different UV amplitudes (the forming force of the active punch was $P(x) = 24$ kN). With the increasing amplitudes, the corresponding bulging radii were measured as 31.95, 32.37, 33.07, and 34.58 mm, and the wall thickness decreased more significantly. This showed that the UV could promote the bulging height and increase the fluidity of the material under the same forming force. As described in Section 4, the amplitudes were varied, and the FE-DE coupled model was established. On comparing the wall thicknesses at the highest point in the experiments

and at the simulated highest point, the relative errors with the increase in amplitude were 0.59%, 1.50%, 2.26%, and 0.87%. The values were all less than 5%. Thus, the variation trend of the wall thickness from the simulations was consistent with that of the experiments.
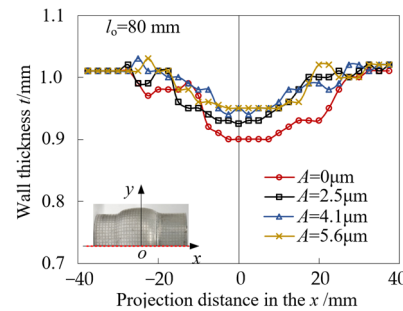

Figure 16. Wall thickness curves under different transverse UV conditions.

The formed tubes are shown in Figure 16. When the forming force was $P(x) = 24$ kN, the indent lengths of the free end for the different amplitudes were 8.80, 10.10, 11.20, and 12.25 mm. This further proved that transverse UV could promote the flow of the material toward the bulging region. In addition, the forming quality could be improved.

5.2.5. The Effect of UV on the Forming Shape

The bulging parts of the tubes under different amplitudes were obtained through experiments, and their contours were measured. The measurement, simulation, and theoretical results were analyzed, the results are shown in Figure 17. It was found that the results of the ABAQUS simulation and test were in good agreement with the parabola geometric model predictions for free deformation by calculating the absolute errors between them, which had values is between 4.9% and 8.1%. This illustrated the accuracy of the parabola model based on the FE-DE coupling model in the simulation process; this method was effective at modeling the complex tubular components and could be used for subsequent analysis.
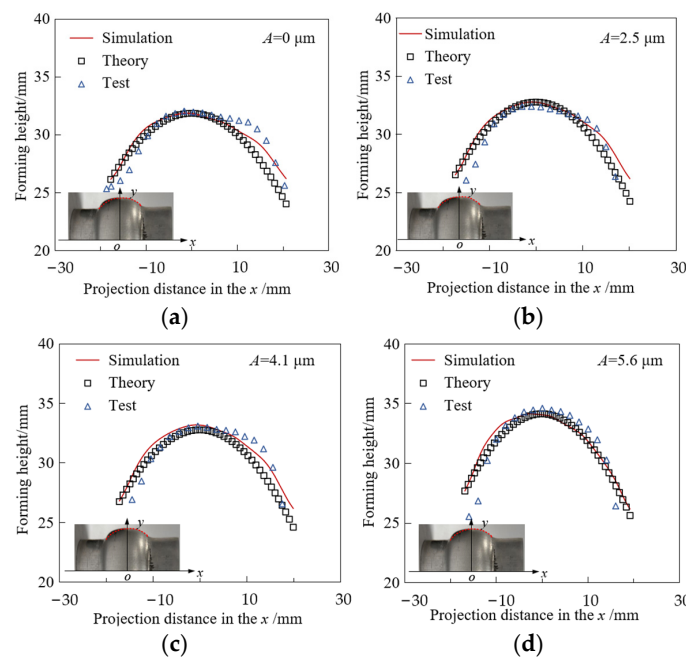

Figure 17. Comparison curve of bulging radius under different *A* values. (**a**) Comparison curve of bulging radius (*A* = 0 μm). (**b**) Comparison curve of bulging radius (*A* = 2.5 μm). (**c**) Comparison curve of bulging radius (*A* = 4.1 μm). (**d**) Comparison curve of bulging radius (*A* = 5.6 μm).

5.2.6. The Effect of UV on the Fracture Morphology

To study the influence of UV on the forming process, the fracture during free expansion of the tube under different amplitudes was analyzed. By analyzing the macroscopic morphological characteristics of the fracture, the macroscopic causes of the failure caused by the UV at different amplitudes were analyzed.

The specimen of the tubular free expansion fracture shown in Figure 18 was observed by scanning electron microscopy (SEM). Microscopic analysis was carried out on the fracture of the tubular material free expansion fracture with a free end for $A = 0$ μm and $A = 5.6$ μm. Two positions were selected that were near and far from the UV, namely A (edge of fracture) and B (center of fracture), and the magnification was 1000 times.
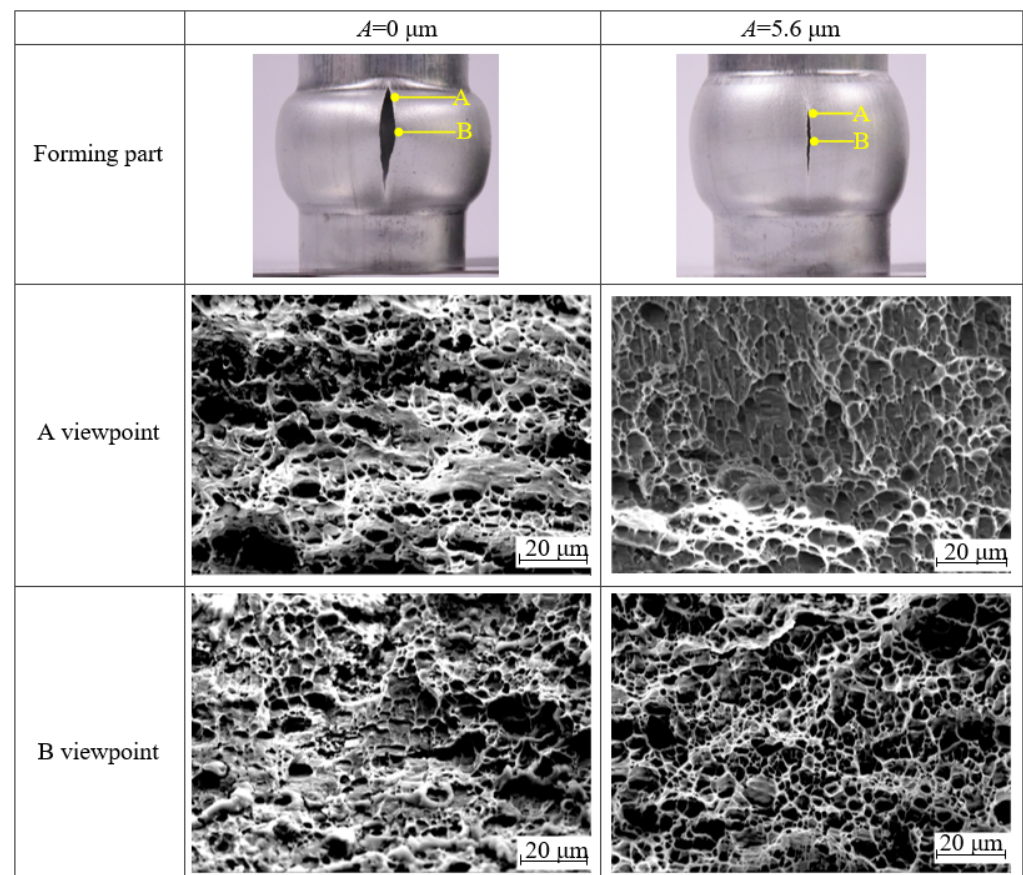

	$A = 0$ μm	$A = 5.6$ μm
Forming part		
A viewpoint		
B viewpoint		

Figure 18. The fracture morphology under different amplitudes.

Based on the deformation at the surface via the orange peel phenomenon, the tube showed the characteristics of plastic fracture. Over time at the different amplitudes, all the fittings reached the limit of rupture, especially in the fracture near the plastic deformation. The rupture line corresponded to uniform axial expansion. The fracture surface was not smooth, indicating that the rupture occurred before the storage of a large amount of energy. The fracture moved farther from the source of the UV with the increase in the amplitude, while it simultaneously became shorter and rougher. The presence of tough nests in the fractures of the tubes at different amplitudes indicated that the 6063-T5 was ductile when it fractured. However, the forming conditions and the shapes of the nests were different at $A = 0$ μm; the nests were parabolic in shape, pointing toward viewpoint B and elongated in the same direction. This indicated that the nests at viewpoint A were formed under tearing stress, whereas at viewpoint B, the nests were formed under different tearing stress. For viewpoint B, there was no evident directionality of the tearing ribs, and it was judged to be an equiaxed tough nest. However, the tough nest size was uneven and small in size, with a reinforcing phase present.

The application of UV (A = 5.6 μm) caused the depth of the ligamentous fossa at viewpoint A near the source to become shallower as the amplitude increased, while the parabolic ligamentous fossa with tearing ribs disappeared; the size of the ligamentous fossa was uniform, and its strengthening phase gradually disappeared. For viewpoint B, the ligamentous fossa had no evident tearing directionality, and the depth of its ligamentous fossa became deeper with the increase in the amplitude, which was significantly larger than that of viewpoint A. The increase in amplitude, therefore, resulted in an increase in plasticity during the forming process and more severe plastic deformation compared to viewpoint A. The tubes reached the forming limit of the material and ruptured. The increase in the amplitude resulted in a gradual reduction in the size of the fracture due to rupture. As the amplitude increased, the further away viewpoint A of the fracture was from the source. Furthermore, the tearing stress gradually disappeared, which laterally indicated that the energy stored before the rupture of the tube was gradually reduced, and therefore, the application of UV also resulted in a reduction in the size of the ruptured fracture.

6. Conclusions

In this paper, a method of applying UV to an SGMF die was proposed. A geometrical model was defined based on the geometric relationship and the state of stress and strain in the tube. Using this model, deformation was studied under different UV amplitudes and frequencies. The application of UV could improve the metal tube flow and increase the fluidity of the granules. The main conclusions are summarized as follows:

(1) To obtain an accurate simulation calculation, the results of the FE-DE coupled method were compared with the results of simulations of the UGMF process performed using ABAQUS 2022 finite element software. In general, within a certain amplitude range, UV could inhibit the thinning of the forming wall and reduce the forming force of the active punch.

(2) Following the simulation results, free bulging tests were carried out, and it was found that the forming force of the active punch decreased as the amplitude of its strokes increased, showing similar results. Therefore, the application of UV could slow down the granule breakage and reduce the thinning of wall thickness.

(3) In the forming process, a parabolic geometric model could accurately describe the radius profile of the free bulging region of the tube. The absolute errors between the simulation and test results were small (within 9%). Therefore, the accuracy of the simulation was verified. At the same time, the accuracy of the FE-DE coupled model under UV was further verified by comparing the wall thickness distribution of the deformation region with that of the simulation.

(4) For the tested 6063-T5 tube, the tearing edge disappeared on the fracture surface when tested at an amplitude of 5.6 μm, and increases in the amplitude caused the fracture size of the tube to gradually decrease. Therefore, the forming amplitude of these tubes benefits from UV, even though higher formability can be achieved at higher amplitudes.

In the future, the UGMF process must be explored thoroughly to further clarify the forming quality as the UV amplitude varies.

Data Availability Statement: The original contributions presented in the study are included in the article. Further inquiries can be directed to the corresponding author.

Conflicts of Interest: The authors declare no conflicts of interest.

References

1. Yang, H.; Li, H.; Zhang, Z.; Zhan, M.; Liu, J.; Li, G. Advances and trends on tube bending forming technologies. *Chin. J. Aeronaut.* **2012**, *25*, 1–12. [CrossRef]
2. Du, Z.H.; Yan, Z.Q.; Cui, X.H.; Chen, B.G.; Yu, H.L.; Qiu, D.Y.; Xia, W.Z.; Deng, Z.S. Springback control and large skin manufacturing by high-speed vibration using electromagnetic forming. *J. Mater. Process. Technol.* **2022**, *299*, 117340. [CrossRef]
3. Reddy, P.V.; Reddy, B.V.; Ramulu, P.J. Evolution of hydroforming technologies and its applications—A Review. *J. Adv. Manuf. Syst.* **2020**, *19*, 737–780. [CrossRef]
4. Bi, J.; Zhao, C.C.; Bi, M.M.; Du, B.; Chen, X.H.; Dong, G.J. Heat treatment and granule medium internal high pressure forming of AA6061 tube. *J. Cent. South Univ. Technol.* **2017**, *24*, 1040–1049. [CrossRef]
5. Chen, H.; Güner, A.; Ben, K.N.; Tekkaya, A.E. Granular media-based press hardening. *J. Mater. Process. Technol.* **2016**, *228*, 145–159. [CrossRef]
6. Ning, F.; Cong, W. Ultrasonic vibration-assisted (UV-A) manufacturing processes: State of the art and future perspectives. *J. Manuf. Process.* **2020**, *51*, 174–190. [CrossRef]
7. Blaha, F.; Langenecker, B. Elongation of zinc monocrystals under ultrasonication. *Die Naturwissenschaften* **1955**, *42*, 556. [CrossRef]
8. Shao, G.; Li, H.; Zhan, M. A review on ultrasonic-assisted forming: Mechanism, model, and process. *Chin. J. Mech. Eng.* **2021**, *34*, 99. [CrossRef]
9. Gao, T.J.; Wang, X.; Liu, S.Q.; Wang, S. Effect of ultrasonic vibration on mechanical properties and bulging performance of TA2 titanium alloy sheet. *Rare Met. Mater. Eng.* **2020**, *49*, 4010–4015.
10. Zhai, J.Q.; Guan, Y.J.; Li, Y.; Liu, Y.; Lin, J. The surface effect of ultrasonic vibration in double cup extrusion test. *J. Mater. Process. Technol.* **2022**, *299*, 117344. [CrossRef]
11. Najafizadeh, N.; Rajabi, M.; Hashemi, R.; Amini, S. A method and apparatus for determination of the ultrasonic-assisted forming limit diagram. *Proc. Inst. Mech. Eng. Part C J. Mech. Eng. Sci.* **2021**, *235*, 7062–7073. [CrossRef]
12. Shahri, S.; Boroughani, S.; Khalili, K.; Kang, B.S. Ultrasonic hydroforming, a new method to improve formability. *Procedia Technol.* **2015**, *19*, 90–97. [CrossRef]
13. Liu, S.; Shan, X.B.; Guo, K.; Yang, Y.C.; Xie, T. Experimental study on titanium wire drawing with ultrasonic vibration. *Ultrasonics* **2018**, *83*, 60–67. [CrossRef] [PubMed]
14. Lin, J.; Pruncu, C.; Zhu, L.H.; Li, J.; Zhai, Y.D.; Chen, L.; Guan, Y.J.; Zhao, G.Q. Deformation behavior and microstructure in the low-frequency vibration upsetting of titanium alloy. *J. Mater. Process. Technol.* **2022**, *299*, 117360. [CrossRef]
15. Kandi, R.; Sahoo, S.K.; Sahoo, A.K. Ultrasonic vibration-assisted turning of Titanium alloy Ti–6Al–4V: Numerical and experimental investigations. *J. Braz. Soc. Mech. Sci. Eng.* **2020**, *42*, 399. [CrossRef]
16. Li, Y.; Zhai, W.D.; Wang, Z.J.; Li, X.Q. Investigation on the material flow and deformation behavior during ultrasonic-assisted incremental forming of straight grooves. *J. Mater. Res. Technol.* **2020**, *9*, 433–454. [CrossRef]
17. Rasoli, M.A.; Abdulla, A.H.; Farzin, M.; Fadaei, T.A.; Taherizadeh, A. Influence of ultrasonic vibrations on tube spinning process. *J. Mater. Process. Technol.* **2012**, *212*, 1443–1452. [CrossRef]
18. Du, B.; Zhao, C.C.; Li, X.F.; He, X. Forming technology of high temperature alloy convex ring shaped by solid granule medium. *Trans. Nonferrous Met. Soc. China* **2014**, *24*, 1721–1729. (In Chinese)
19. Zhang, Y.M.; Proust, G.; Retraint, D.; Retraint, D.; Wang, H.M.; Gan, Y.X. Discrete element simulation of surface mechanical attrition treatment with rough-surface sonotrode. *Int. J. Mech. Sci.* **2019**, *161*, 105060. [CrossRef]
20. Chavoshi, S.Z.; Jiang, J.; Wang, Y.; Fang, S.; Wang, S.Y.; Shi, Z.S.; Lin, J.G. Density-based constitutive modelling of P/M FGH96 for powder forging. *Int. J. Mech. Sci.* **2018**, *138*, 110–121. [CrossRef]
21. Singh, A.; Magnanimo, V.; Saitoh, K. Effect of cohesion on shear banding in quasistatic granular materials. Effect of cohesion on shear banding in quasistatic granular materials. *Phys. Rev. E* **2014**, *90*, 022202. [CrossRef] [PubMed]
22. Barreto, D.; O' Sullivan, C. The influence of inter-particle friction and the intermediate stress ratio on soil response under generalised stress conditions. *Granul. Matter* **2012**, *14*, 505–521. [CrossRef]
23. Liu, H.; Zhang, S.H.; Song, H.W.; Shi, G.L.; Cheng, M. 3D FE-DE coupling analysis for granular-media-based thin-wall elbow push-bending process. *Int. J. Mater. Form.* **2019**, *12*, 985–994. [CrossRef]
24. Marini, M.; Piona, F.; Fontanari, V.; Bandini, M.; Benedetti, M. A new challenge in the DEM/FEM simulation of the shot peening process: The residual stress field at a sharp edge. *Int. J. Mech. Sci.* **2020**, *169*, 105327. [CrossRef]
25. Khasanov, O.L.; Dvilis, E.S. Net shaping nanopowders with powerful ultrasonic action and methods of density distribution control. *Adv. Appl. Ceram.* **2008**, *107*, 135–141. [CrossRef]
26. Cao, M.Y.; Hu, H.; Jia, X.D.; Han, X.B.; Yao, P.L. FE-DE coupling analysis of AZ31B sheet solid granule medium forming based on GTN model. *Int. J. Adv. Manuf. Technol.* **2020**, *111*, 1617–1626. [CrossRef]
27. Song, H.W.; Xie, W.L.; Zhang, S.H.; Jiang, W.H.; Lăzărescu, L.; Banabic, D. Granular media filler assisted push bending method of thin-walled tubes with small bending radius. *Int. J. Mech. Sci.* **2021**, *198*, 106365. [CrossRef]
28. Redwood, M. *Mechanical Waveguide*; Pergamon Press: Oxford, UK, 1960.
29. Lee, H.; Singh, R. Acoustic radiation from out-of-plane modes of an annular disk using thin and thick plate theories. *J. Sound Vib.* **2005**, *282*, 313–339. [CrossRef]

30. Ludwikson, D.C. Modified stress-strain relation for FCC metals and alloys. *Metall. Trans.* **1971**, *2*, 2825–2828. [CrossRef]

31. Simulia, D. *Abaqus 6.14 Analysis User's Manual*; Dassault Systèmes Simulia Corp.: Providence, RI, USA, 2014.

32. Cao, M.Y.; Li, J.C.; Liu, Y.Y.; Yuan, Y.N.; Zhao, C.C.; Dong, G.J. Frictional characteristics of sheet metals with superimposed ultrasonic vibrations. *J. Cent. South Univ.* **2018**, *25*, 1879–1887. [CrossRef]